PROCEEDINGS OF SPIE

SPIEDigitalLibrary.org/conference-proceedings-of-spie

Maskless nanolithography on the basis of microfocus x-ray tubes: conversion of electron energy into the BeKα line

N. I. Chkhalo, A. Ya. Lopatin, A. E. Pestov, N. N. Salashchenko, G. D. Demin, et al.

N. I. Chkhalo, A. Ya. Lopatin, A. E. Pestov, N. N. Salashchenko, G. D. Demin, N. A. Dyuzhev, M. A. Makhiboroda, "Maskless nanolithography on the basis of microfocus x-ray tubes: conversion of electron energy into the BeKα line," Proc. SPIE 11022, International Conference on Micro- and Nano-Electronics 2018, 110221M (15 March 2019); doi: 10.1117/12.2522105

SPIE.

Event: The International Conference on Micro- and Nano-Electronics 2018, 2018, Zvenigorod, Russian Federation

Downloaded From: https://www.spiedigitallibrary.org/conference-proceedings-of-spie on 03 Apr 2019 Terms of Use: https://www.spiedigitallibrary.org/terms-of-use

Maskless nanolithography on the basis of microfocus X-ray tubes: conversion of electron energy into the BeKα line

N.I. Chkhalo[a], A.Ya. Lopatin*[a], A.E. Pestov[a], N.N. Salashchenko[a], G.D. Demin[b], N.A. Dyuzhev[b], M.A. Makhiboroda[b]
[a]Institute for physics of microstructures RAS, GSP-105, Nizhny Novgorod, Russia; [b]National University Research Institute of Electronic Technology, Zelenograd, Russia

ABSTRACT

The article describes the status of work on the project of maskless x-ray nanolithography using a chip of transmission microfocus X-ray tubes with field emission cathodes as a dynamic mask device. The basic principles of this method of projection photolithography are considered, and the estimations of the expected throughput of the process are given. A noticeable part of the article is devoted to a model for numerical simulation of the emission characteristics of thin film targets at their exitation with a low energy electrons beam. The experimental results on measurements of the conversion efficiency of electrons energy into soft X-ray radiation of berillium Kα line (λ=11.4 nm) are presented. Other promising materials which could be used as efficient film targets for the mentioned design of maskless nanolithography are proposed.

Keywords: extreme ultraviolet radiation, projection photolithography, dynamic mask, field emission nanocathode, conversion efficiency

1. INTRODUCTION

Projection photolithography is a key technology of microelectronics, which determines the process node of integrated circuits. The smallest achieved technology nodes of 10 nm and 7 nm use deep UV immersion photolithography at a wavelength of 193 nm or EUV lithography at a wavelength of 13.5 nm[1-2]. The most complex and expensive elements of the infrastructure of projection lithography are masks. The price of only one set of masks may be as much as several million dollars. Because of expensive masks, along with a high cost and complexity of the equipment, the projection photolithography becomes competitive at mass-production only - it doesn't meet the demands of small and middle volume manufacturing. Thus, the proposition and development of new tools for high resolution nanolithography remains an actual task.

The hypothetical nanolithographer should provide a spatial resolution within a range of 100 - 10 nm and have the throughput of one to three orders of magnitude lower than the throughput of existing industrial tools of projection photolithography. No static masks should be used in order to obtain the process cost which will be practically independent on the volume of production. The principle of dynamic mask formation can be involved to solve this problem. The important notice is that the proposed nanolithographer has to be comparable in cost with a one-beam tool of electron nanolithography, being at the same time much more advantageous in productivity. In this case it will be possible to state that the manufacturing of nanoelectronics is affordable not only to global factories, but also to smaller companies and research institutes, giving an additional impetus for the development of nano-sized integrated circuits.

Proposals for the development of the schemes of maskless photolithography with exposure to radiation of SXR (soft X-ray) and EUV ranges began to appear already at the end of the last century. Approximately in the same years, a cycle of successful works on contact lithography in SXR range was performed, demonstrating resolution on a photoresist of several tens of nanometers[3-4], which could not be technically realized at that time using longer wavelength UV radiation. One of the discussed schemes for maskless exposure[5] concluded in the usage of a matrix of transmission type Fresnel zone plates to form a matrix of focal spots directly on a photoresist coated wafer. The achievable spatial resolution of this scheme, determined by the focal spot size, is comparable with the minimum width of the Fresnel plate zone. If it is

*lopatin@ipm.sci-nnov.ru

International Conference on Micro- and Nano-Electronics 2018, edited by Vladimir F. Lukichev, Konstantin V. Rudenko, Proc. of SPIE Vol. 11022, 110221M · © 2019 SPIE
CCC code: 0277-786X/19/$18 · doi: 10.1117/12.2522105

Downloaded From: https://www.spiedigitallibrary.org/conference-proceedings-of-spie on 03 Apr 2019
Terms of Use: https://www.spiedigitallibrary.org/terms-of-use

necessary to increase the resolution, the scheme can be supplemented with a projection lens that will form a demagnified image of the illumination distribution formed by zone plates. Calculations show that a projection lens of two aspherical mirrors with a numerical aperture NA = 0.3 and 10-fold demagnification can provide the diffraction limit of resolution (about 22 nm for a wavelength of 13.5 nm) in an area with the size of more than 10 mm[6]. The concept of a dynamic mask using zone plates was implemented as an exposure tool operating in UV spectral region[7]. In our opinion, the possibility of the rapid implementation of the proposed concept in EUV range is doubtful since technological approaches to the fabrication of a matrix consisting of a significant number of zone plates with individual optical shutters remain unclear. Another proposal[8] was to use the projection scheme with a dynamic mask in the form of a matrix of micromirrors allowing tilting of each mirror element. At present time the production of such kind of dynamic mask chips using MEMS technology is well developed. The possibility to deposit onto the surface of the chip zero-stress multilayer coating with a reflectivity of about 40% at a wavelength of 13.5 nm was experimentally demonstrated[9]. The estimations show[10] that the throughput of EUV lithography tool with a micromirrors based dynamic mask can be comparable to the throughput of the tool with conventional masks. However, since the size of the mirror elements of commercially available MEMS is not less than several micrometers, the practical implementation of the aforesaid scheme will not be able to maintain today's norms of spatial resolution.

Eventually, the projects of multi-beam electron lithography were admitted as the most promising for the implementation of the idea of high resolution maskless lithography, in particular, the project of Mapper Lithography company[11]. The throughput of already built tools of electron exposure can reach several 300-mm wafers per hour at the technology node of 28 nm. Plans are announced for the manyfold increase in productivity when clustering several identical lithographic modules. But it should be noted that according to the specification given on the company's website[12] the losses of electrons at the formation of individual beamlets are very large: only 17 μA of current reaches the wafer level at an initial electron gun current of 100 mA.

The low efficiency of using of an electron source in the tools of multi-beam electron lithography, which is comparable to the efficiency of generation of characteristic X-ray lines at electron exciting of solid targets, leaves a chance for the development of the systems of maskless SXR and EUV nanolithography with X-ray tube in the role of a radiation source. In ref.[13] we proposed a variant of such a system in which the functions of a dynamic mask are fulfilled by an integrated circuit of microfocus X-ray tubes with a thin film transmission type target. Estimates of its performance are given in ref.[14]. The present article discusses the basic principles of this lithography method, describes the technique for manufacturing thin film beryllium targets, gives the results of calculations and measurements of the conversion efficiency of electrons energy into BeKα characteristic line (λ = 11.4 nm) as well as the results on energetic spectra of transmitted electrons. Alternative wavelengths (and, thus, target materials) are suggested to be tested.

2. PRINCIPLE OF OPERATION

The scheme of the proposed method of maskless lithography based on the integrated circuit of microfocus X-ray tubes is shown in Fig. 1. The basic idea consists in the use of silicon chips of pointlike field emission cathodes integrated with modulating electrodes. The technology for manufacturing such chips is currently well developed, and the prospectives of their application for hard X-ray generation are experimentally demonstrated[15-16]. The principle of operation of the scheme is as follows. DC positive voltage in the range of 0.5 - 4 kV is applied between the film target and the common electrode of field emission nanocathodes. At the same time, negative bias voltage is applied to modulating electrodes in order to supress the electron emission. As the potentials of modulating electrodes are controlled separately, the decrease of the bias voltage of some individual emitter will switch on the corresponding electron beam falling onto the target. X-ray emission will be generated from the target. At high electron currents the target will undergo large heat loads, so that the heat sink through the chip to an active cooling system, which is not shown in Fig. 1, will be present in practical design. From the point of view of applicability of this radiation source for the purposes of high resolution lithography, the sizes of the emission spots have to be as small as possible. It's planned to be achieved, firstly, owing to the usage of soft X-ray characteristic radiation of low-Z materials. The reason is that SXR radiation may be generated at rather low energy of incident electrons resulting in the limitation of the source size in depth of the film target. Beryllium is now considered as one of prospective target materials with a Kα line of 11.4 nm. Secondly, both the short distance to the target and the focusing action onto electrons of the electrical field of a modulating electrode have to confine a spot size in the transverse direction. Thus, a matrix source of soft X-ray radiation with sub-micron pixel size will be obtained, the state of pixels of which can be controlled by a computer. Similar approach in UV range was reported in[17] - the light source and the mask were combined in one matrix of leds. The image of the source is then transferred to the resist coated

Downloaded From: https://www.spiedigitallibrary.org/conference-proceedings-of-spie on 03 Apr 2019
Terms of Use: https://www.spiedigitallibrary.org/terms-of-use

wafer by means of two-mirror optical system with 10x demagnification. Though a matrix of nanocathodes itself could be of significant interest as a promising source for multi-beam electron lithography, we do not consider the additional conversion of the electron energy into SXR radiation just as undue losses. The advantages are potentially higher spatial resolution, practical absence of the problems of interbeam interaction and of charge accumulation, and generally more flexible architecture.

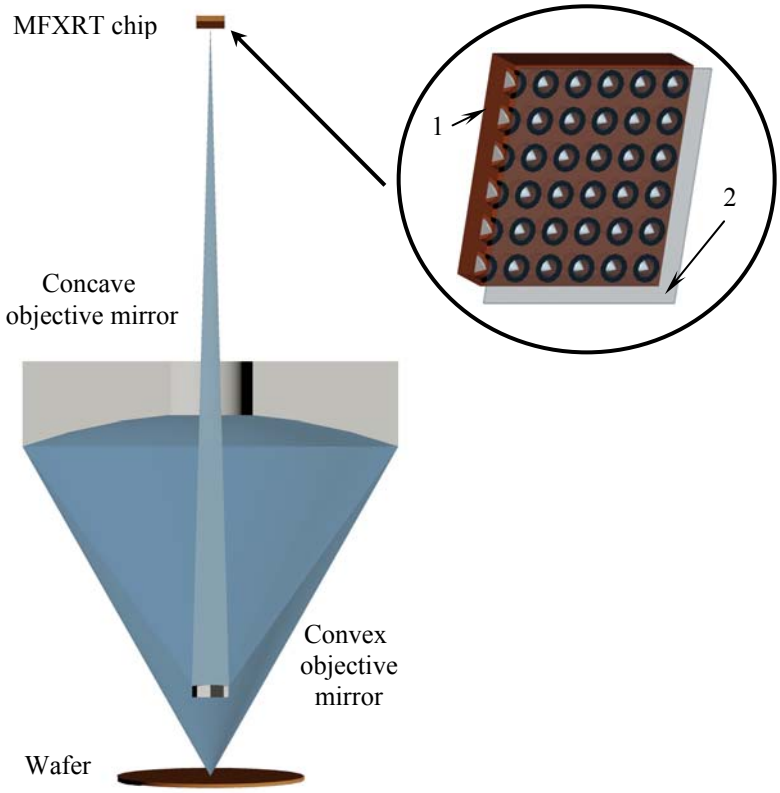

Figure 1. Layout of the system of maskless nanolithography on the basis of microfocus X-ray tubes (MFXRT). In the tab - schematic representation of MFXRT chip: 1 - a matrix of field emission nanocathodes, 2 - thin film target.

In order to estimate the throughput of the lithographic process, the expression derived in ref.[14] has to be applied:

$$PLP = \frac{P_e \cdot CE \cdot NA^2 \cdot R^2}{4 \cdot S \cdot M^2} \qquad (1)$$

where PLP is the throughput, P_e is the power of the electron beam, CE is the conversion coefficient of the electron beam to the energy of characteristic radiation emitted to the solid angle 4π, NA is the numerical aperture, R is the reflectivity of each of two mirrors, M is the demagnification, and S is the resist sensitivity. If we'll insert the achieved value of an average current density[15] of 1 A/cm^2, which corresponds to P_e = 1 kW at an accelerating voltage of 1 kV and a source size of 1 cm^2, the achieved reflectivity of Mo/Be multilayer mirror at λ = 11.4 nm of 70%[18-19], NA = 0.5, M = 10, S = 10 mJ/cm^2, and a value of fluorescence yield in 4π solid angle[20] of $3.6 \cdot 10^{-4}$ taken as an estimation of CE, the formula (1) will give the expected value of $PLP \approx 40$ cm^2 per hour. Though this level of productivity is 3 orders of magnitude lower than one of the industrial tools for EUV projection lithography, it still remains about 3 orders higher than the productivity of a typical alone e-beam lithography scheme[21]. The necessity of more precise knowledge of the conversion efficiency and of its dependence on such parameters as the film thickness and the energy of incident electrons inspired us to fulfill detailed investigation of this item – both theoretical and experimental.

Downloaded From: https://www.spiedigitallibrary.org/conference-proceedings-of-spie on 03 Apr 2019
Terms of Use: https://www.spiedigitallibrary.org/terms-of-use

3. NUMERICAL SIMULATION

3.1 Model of electron interaction with a film target

Emission of radiation from X-ray tubes is a result of a random process of multiple interactions of an electron with target atoms. Such processes can be described using the Monte Carlo method. In this method the electron trajectory is represented as a sequence of elastic collisions with the nuclei of atoms and inelastic collisions with the electron shells. It's assumed that at each collision an electron interacts with only one atom. The distance between two successive interactions is characterized by the mean free path ζ. At each step, the angle between the previous and next directions of electron velocity θ, the azimuth angle φ and the angle between the velocity direction and the normal to the target surface β are determined. The electron trajectory is a broken line in this consideration. The type of each collision is played out taking into account the ratio of total cross-sections for elastic and inelastic processes. Collisions are classified in dependence on the final state of the atom. At an inelastic collision the atom is either excited or ionized. At an elastic collision the atom remains in the same state, but an electron loses some part of energy due to bremsstrahlung. In the first case the characteristic photon is then emitted with a probability equal to a radiative yield. In the second case an emitted photon belongs to continuous spectrum. The general calculation scheme in the proposed model includes sequental playouts of the following: the type of collision, the loss of electron energy, the scattering angle, the azimuthal angle, the mean free path. Physical data of berillium necessary for the calculation such as, in particular, the modeled K-level ionization cross-section[22], the total elastic and inelastic cross-sections[23], optical constants[24] and the radiative yield[20] were taken from the literature. A more detailed description of the model is given in our former work[25], where the Monte Carlo method was applied to predict the conversion efficiency of the electron energy into the energy of BeKα line for a case of transmission type film targets.

3.2 Calculation of the conversion efficiency

The spectra of X-ray radiation of Be target were simulated at the normal incidence of the exciting electron beam for various accelerating voltages in the range of 0.5 - 10 kV and various target thicknesses from 20 nm to 650 nm. A typical calculated spectrum derived at an electron current of 1 A is shown in Fig. 2a. Here the accelerating voltage and the film thickness were taken to be 5 kV and 200 nm, respectively. It can be seen that the spectrum represents a combination of the characteristic radiation and the bremsstrahlung. The intensity of the line of 11.4 nm is much higher than the bremsstrahlung background that is typical for low-Z elements.

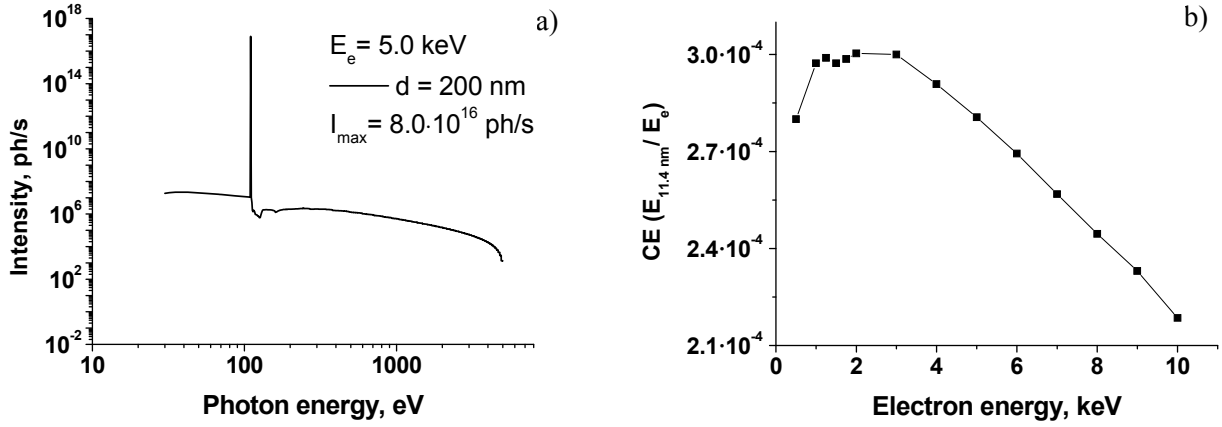

Figure 2. a) Simulated spectrum of 200 nm thick Be target at an accelerating voltage of 5 kV; b) conversion efficiency to the solid angle 4π of electron energy to an emission line of 11.4 nm calculated for an optimal target thickness in the transmission geometry.

The dependence of the calculated conversion efficiency on the electron energy is presented in Fig. 2b. A plateau on this curve corresponds to the electron energy range of 1 – 3 keV, being consistent with the theoretical concept[26] that the maximal emission efficiency takes place at electron energies of the order of ten ionization potentials. The efficiency is calculated for optimal thicknesses of the target which lay within the range 50 – 100 nm for the electron energies of 1 - 3 kV.

Downloaded From: https://www.spiedigitallibrary.org/conference-proceedings-of-spie on 03 Apr 2019
Terms of Use: https://www.spiedigitallibrary.org/terms-of-use

3.3 Energy spectra of transmitted electrons

In order to study the process of interaction of accelerated electrons with matter in more details, in particular, to revise total interaction cross-sections at comparison of simulation results with experimental ones, the energy spectrum of electrons transmitted through the target was calculated. The calculation was carried out for films with a thickness of 100, 200, 300 and 400 nm. An example of the spectra of transmitted electrons for two different thicknesses and several values of the energy of the incident electrons is shown in Fig.3.

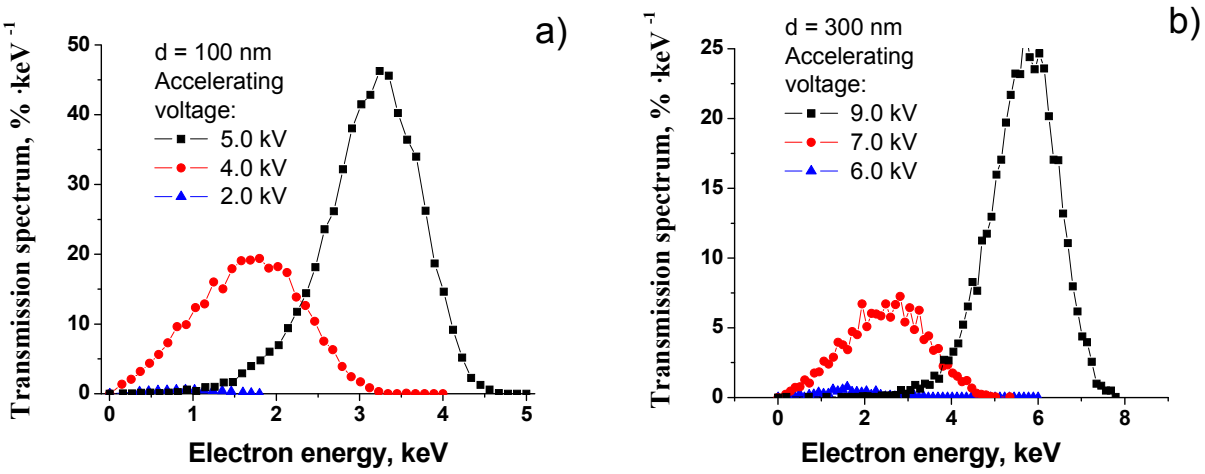

Figure 3. Simulated energy spectrum of transmitted electrons for several values of accelerating voltage. The thickness of Be film is 100 nm (a) and 300 nm (b).

4. EXPERIMENT

4.1 Target fabrication

Beryllium film targets were fabricated using the technique of magnetron sputtering of Be layers onto silicon substrates with preliminary deposited sacrificial layer. The sacrificial layer has to be chosen in such a way that it might be dissolved during liquid etching while keeping intact the main Be layer. In our case magnesium sub-layer was used for this purpose in a pair with acetic acid as an etching agent. The samples of film targets for experimental studies were manufactured with the thicknesses of 100, 200, 300 and 400 nm and a diameter of all freestanding films of 10 mm. A set of samples of each thickness was fabricated using the option of group fabrication and the design of stretched membranes, as it was described in details in ref.[27].

4.2 Scheme of the experimental bench

In experiments on the interaction of accelerated electrons with a film Be target the samples of films have been mounted onto a holder inserted into a vacuum chamber through the flange. In the same chamber the electron gun with a filament cathode was placed in the front of the target, and either the X-ray detector assembly for emission measurements or the Faraday cup for measurements of transmitted electrons could be disposed behind the target. The electron beam from the cathode were pulled out with an accelerating electrode and then focused with a solenoid lens onto the film target with a spot size of about 2 mm. The target was grounded through the current sensing resistor. Soft X-ray emission was detected with the help of an absolutely calibrated silicon photodiode described elsewhere[28]. An additional 200 nm thick Be filter was installed between the target and the detector to suppress long wavelength background. Its transparency was about 80% at a wavelength of 11.4 nm and $5.6 \cdot 10^{-6}$ at $\lambda = 633$ nm so that the suppression of visible light of the filament was not lower than 5 orders of magnitude. Since the bremsstrahlung radiation for such low-Z material as Be is expected to be several orders of magnitude weaker than the characteristic one all the detected signal was supposed to be the signal of a characteristic line BeKα ($\lambda = 11.4$ nm). At the measurements of the energy distribution of transmitted electrons the Faraday cup was used instead of X-ray detector. Data were derived from the dependencies of the collected current on the repulsive potential of the grid positioned in the front of the collector. The photo of the bench is shown in Fig. 4.

Downloaded From: https://www.spiedigitallibrary.org/conference-proceedings-of-spie on 03 Apr 2019
Terms of Use: https://www.spiedigitallibrary.org/terms-of-use

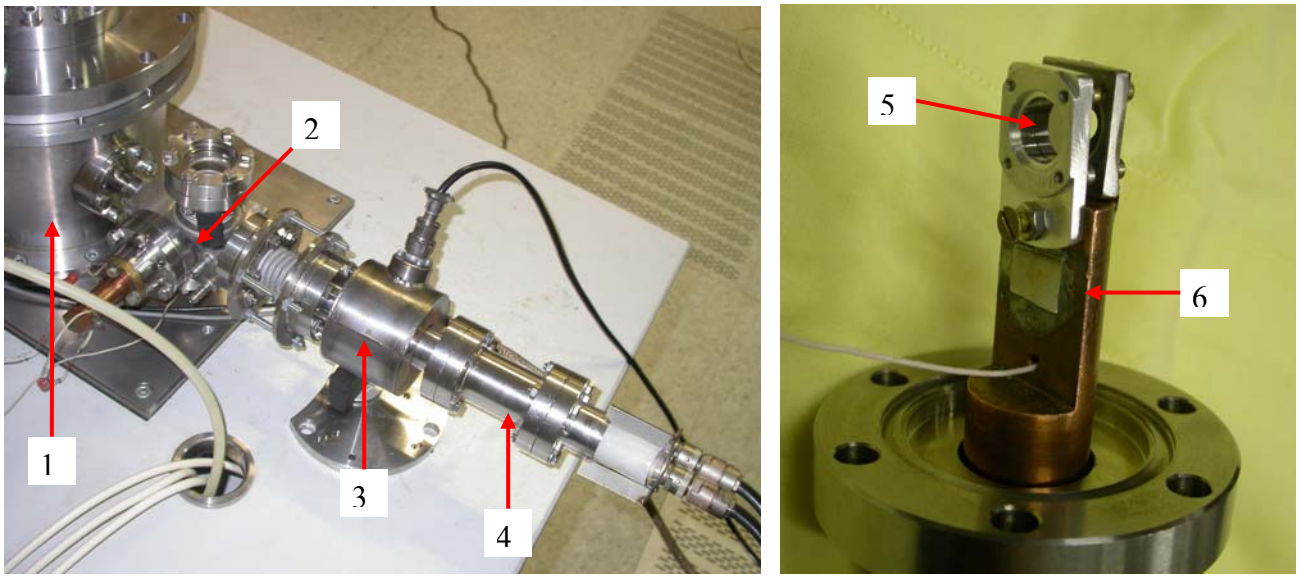

Figure 4. Photograph of the fragment of the experimental bench (a) and of the target mount (b). Simulated energy spectrum of transmitted electrons for several values of accelerating voltage. The thickness of Be film is 100 nm (a) and 300 nm (b). 1 - the chamber of X-ray detector / Faradey cup; 2 - the chamber of film target; 3 - solenoid lens; 4 - filament assembly; 5 - transmission type film target; 6 - target holder.

4.3 CE measurements

In the experiment for measurements of the conversion efficiency (CE) the signal from the target was recorded depending on the accelerating voltage, and the current of electrons to the target was measured simultaneously. From this data the conversion efficiency to the solid angle 2π of the electron energy to the energy of a characteristic line BeKα was calculated by the formula:

$$CE_{2\pi} = \frac{P_{ph} \cdot 2\pi}{P_e \cdot \Omega_d} \tag{2}$$

where $\Omega_d = 2.6 \cdot 10^{-3}$ is the reception solid angle of the detector, P_{ph} is the radiation power falling onto the detector, P_e is the power of the electron beam. The power of photons registered by the detector is proportional to the photodiode current as follows:

$$P_{ph} = \frac{I_d}{S_d \cdot T_f} \tag{3}$$

where I_d is the detector current in amperes, $S_d = 0.23$ A/Watt is the detector sensitivity at $\lambda = 11.4$ nm[28], and T_f is the filter transparency.

Two factors have to be taken into account at processing of experimental data. The first one is that the conversion efficiency can differ from the value given by expression (2) since we didn't study the angular distribution of the emission in this work. We could expect a slight decrease in radiation output moving away from the target normal. The second one is that the data becomes not valid at rather high accelerating voltages, at which the significant amount of electrons pass through the target almost with no scattering. Low divergent electron beam hit beryllium filter of the detector assembly in these conditions. It generates X-ray emission from the filter observed as a rapid growth of the diode current.

Examples of the experimental dependencies of the detector signal and CE on the accelerating voltage are presented in Fig. 5. The maximum value of the measured conversion efficiency to a solid angle of 2π was found to be $4.6 \cdot 10^{-5}$ for a 200 nm thick Be film and an electron energy of 2.75 keV. This value is about three times smaller in comparison with the simulation result.

Downloaded From: https://www.spiedigitallibrary.org/conference-proceedings-of-spie on 03 Apr 2019
Terms of Use: https://www.spiedigitallibrary.org/terms-of-use

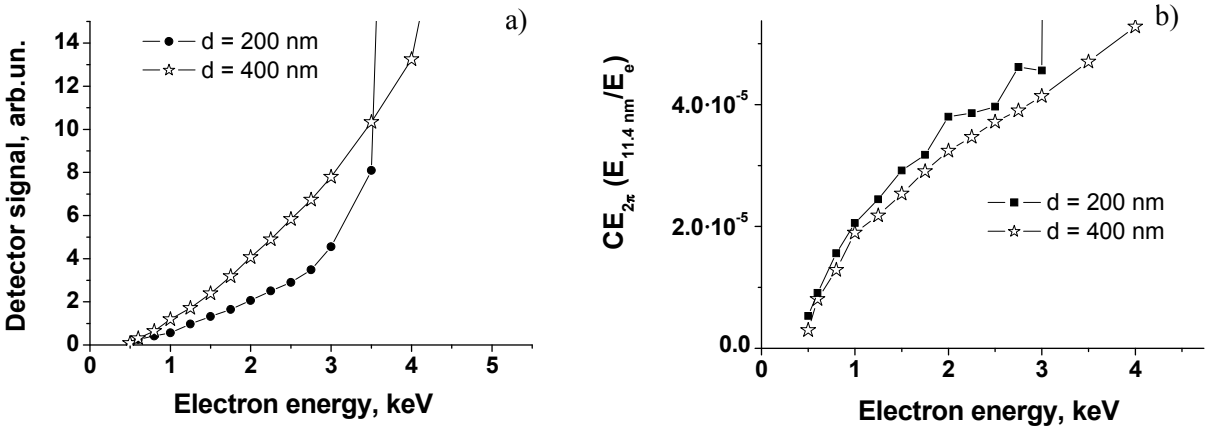

Figure 5. X-ray detector signal (a) and obtained conversion efficiency (b) in dependence on the energy of incident electrons. Experimental curves for are shown for 200 nm and 400 nm thick Be targets.

4.4 Measured electron energy spectra

From the point of view of the technical complexity the measurements of the electron spectra represented simpler task as compared to CE measurements. The reason is that rather high currents of incident electrons had to be used to certainly detect X-ray signal. The currents were in the range 10 – 20 μA at measurements of the emission, causing strong heating of the film target to more than 500°C at intensities of heat loads of 1.5 – 2 W/cm^2. At the measurements of transmitted electrons the incident current and, thus, the heating were reduced to the safe level. The energy spectra of transmitted electrons were experimentally studied for the thicknesses of the target 100 nm and 300 nm (Fig. 6). Exactly as in the case of measuring conversion efficiency, absolute values along the y-axis in Fig. 6 are assigned in an assumption of isotropic electron distribution in the solid angle 2π.

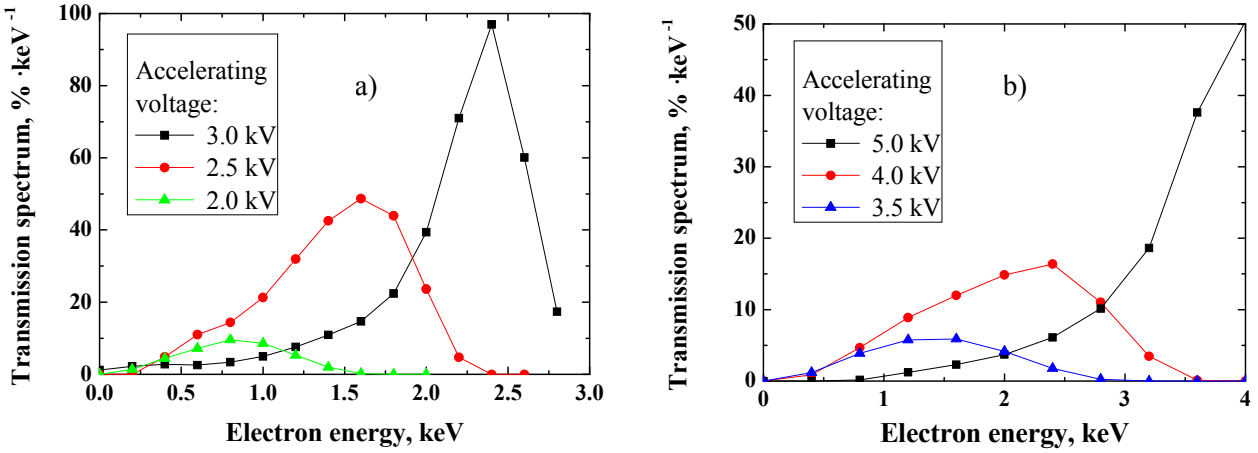

Figure 6. The experimental energy spectra of transmitted electrons built for various accelerating voltages and for Be target thickness of 100 nm (a) and 300 nm (b).

5. DISCUSSION AND CONCLUSION

There is an impressive quantity of works devoted to the simulation of the emissive characteristics of X-ray tubes. In particular, a number of software products are available via the Internet[29-31]. However, these programs either have no data on the emission lines of low-Z elements or refer to semi-empirical cross-sections which can be considered as sufficiently reliable for the atomic number Z>6. Moreover, ready software solutions usually don't allow making a calculation for the transmission geometry: the radiation is assumed to be emitted to the same half-space where electrons

Downloaded From: https://www.spiedigitallibrary.org/conference-proceedings-of-spie on 03 Apr 2019
Terms of Use: https://www.spiedigitallibrary.org/terms-of-use

are falling from. In our present work an attempt of the numerical simulation was undertaken to predict the emission intensity from the transmission type thin film Be target. Relatively recent data on the ionization cross-section of beryllium[22] was chosen for Monte Carlo modeling.

Owing to the progress in the manufacturing of freestanding Be films with the exactly controlled thickness in the range from a hundred to several hundreds of nanometers, it became possible to compare the calculation results with the reliable experimental data. It was found that currently the model can not give an adequate description of the experiment. The calculated value of the maximum conversion efficiency of the electron energy into the energy of BeKα line over the solid angle 4π is $3.0 \cdot 10^{-4}$, almost achieving the value of the fluorescence yield $\omega_K = 3.6 \cdot 10^{-4}$ reported in ref.[20]. It corresponds to the case when the main amount of electron energy is spent in inelastic collisions; the bremsstrahlung contribution is strongly suppressed. Direct measurements gave the CE value which is smaller about thrice. There is also a large discrepancy between simulated and experimental spectra of transmitted electrons. The electron beam begins to penetrate through the film at much lower energies than it is predicted by our calculations. Obviously, the ionization cross-section[22] used for the calculation turned out to be overdrawn and needs to be corrected.

Coming back to the main idea of the present report – the idea of maskless nanolithography on the basis of microfocus X-ray tubes – the forecast of the throughput from section 2 has now to be revised, namely, the expected throughput should be reduced approximately in three times to a new value of $PLP \approx 13$ cm^2 per hour. In our opinion, such level of productivity is still interesting for the prototyping of nanoelectronic devices and even for low volume manufacturing. The supplemental reserves for some growth of the productivity are the decrease of demagnification M of the mirror objective and the scaling of the electron power with the size of the chip of microfocus tubes. The first of these two steps will be possible in the case of success in the decrease of the pixel size of the chip. The second one will depend on the development of effective cooling system.

One more possibility to improve the performance of the proposed method of nanolithography is further optimization of the film target. In relation to beryllium based targets the study of multilayer films with interlayers of heavy metals is planned. Presumably, the electron deceleration in dense interlayers could lead to the increase of CE in the range of large electron energy, in which films of pure beryllium become transparent to electrons. The study of other target materials, above all, of ones with a high fluorescence yield is also has to be scheduled. Characteristics of some promising materials in conjunction with the experimentally obtained reflectivity and spectral selectivity of the appropriate X-ray mirrors are given in Table 1. In this table the central column refers to the fraction of characteristic line energy within the spectral band of reflectivity of two-mirror objective. The rightmost column represents estimated relative productivity of the system with a target made of specified material.

Table 1. X-ray emission lines and fluorescence yield ω of some materials[20]; optical properties of appropriate mirrors.

Material	λ, nm	ω	f	R	Δλ, nm	ω×f×R^2
Si	13.5	$3.8 \cdot 10^{-4}$	0.36	0.7	0.53	$0.67 \cdot 10^{-4}$
Be	11.4	$3.6 \cdot 10^{-4}$	0.66	0.7	0.40	$1.16 \cdot 10^{-4}$
B	6.76	$5.6 \cdot 10^{-4}$	0.28	0.64	0.06	$0.64 \cdot 10^{-4}$
C	4.47	$26 \cdot 10^{-4}$	0.09	0.2	0.025	$0.09 \cdot 10^{-4}$
N	3.16	$50 \cdot 10^{-4}$	1	0.25	0.011	$3.13 \cdot 10^{-4}$
Ti	3.136	$17 \cdot 10^{-4}$	1	0.25	0.011	$1.06 \cdot 10^{-4}$
Sc	3.135	$10 \cdot 10^{-4}$	1	0.25	0.011	$0.62 \cdot 10^{-4}$

As it can be seen, nitrogen containing targets seem the most promising from the point of view of both the expected throughput and the achievable spatial resolution of the lithography process. Nitrogen containing films for further experiments will be fabricated in the form of compounds – nitrides of titanium or scandium.

ACKNOWLEDGMENTS

The facilities of the center of collective use “Microsystems technology and electronic component base” (MIET) were used to fulfill this work. The work was financially supported by Russian Ministry of Education and Science within the frame of the Agreement №14.578.21.0250 (RFMEFI57817X0250). The work was also sponsored by the following grants: RSCF №17-12-01227 in the part of experimental investigation, RFBR №18-42-520007 in the part of Be film samples fabrication, and RFBR №18-02-00173 in the part of the development of the electron gun for our research.

Downloaded From: https://www.spiedigitallibrary.org/conference-proceedings-of-spie on 03 Apr 2019
Terms of Use: https://www.spiedigitallibrary.org/terms-of-use

REFERENCES

[1] Jones, S., "TSMC's 10 nm process offers the highest transistor density," https://seekingalpha.com/article/4151376-tsmc-intel-lead-semiconductor-processes (27 February 2018).

[2] Kim, S.-S., Chalykh. R., Kim, H., Lee, S., Park, Ch., Hwang, M., Park, J.-O., Park, J., Kim, H., Jeon, J., Kim, I., Lee, D., Na, J., "Progress in EUV lithography toward manufacturing," Proc. SPIE 10143, 1014306 (2017).

[3] Vladimirsky, Y., Bourdillon, A., Vladimirsky, O., Jiang, W. and Leonard, Q., "Demagnification in proximity x-ray lithography and extensibility to 25 nm by optimizing Fresnel diffraction", J. Phys. D: Appl. Phys. 32(22), L114 (1999).

[4] Bourdillon, A. J., Boothroyd, C. B., Kong, J. R. and Vladimirsky, Y., "A critical condition in Fresnel diffraction used for ultra-high resolution lithographic printing", J. Phys. D: Appl. Phys. 33(17), 2133-2141 (2000).

[5] Smith, H. I., "A proposal for maskless, zone-plate-array nanolithography", J. Vac. Sci. Technol. B 14(6), 4318 - 4322 (1996).

[6] Johnson, K. C., "Scanned-spot-array extreme ultraviolet imaging for high-volume maskless lithography", J. Vac. Sci. Technol. B 30(5), 051606 (2012).

[7] https://www.lumarray.com/products.htm

[8] Choksi, N., Pickard, D. S., McCord, M., Pease, R. F. W., Shroff, Y., Chen, Y., Oldham, W., Markle, D., "Maskless extreme ultraviolet lithography," J. Vac. Sci. Technol. B 17(6), 3047-3051 (1999).

[9] Chkhalo, N., Polkovnikov, V., Salashchenko, N., and Toropov, M., "Deposition of Mo/Si multilayers onto MEMS micromirrors and its utilization for extreme ultraviolet maskless lithography," J. Vac. Sci. Technol. B, 35, 062002 (2017).

[10] Chkhalo, N. I., Polkovnikov, V. N., Salashchenko, N. N., Toropov, M. N., "Problems and prospects of maskless (B)EUV lithography," Proc. of SPIE, 10224, 102241O-1-O8 (2016).

[11] Servin, I., Thiam, N. A., Barros, P.-P., Pourteau, M.-L., Mebiene, A.-P., Jussot, J., Pradelles, J., Essomba, Ph., Lattard, L., Brandt, P., Wieland, M., "Ready for multi-beam exposure at 5kV on MAPPER tool: Lithographic & process integration performances of advanced resists/stack," Proc. SPIE 9423, 94231C (2015).

[12] https://mapper.nl/company

[13] Dyuzhev, N. A., Demin, G. D., Gryazneva, T. A., Pestov, A. E., Salashchenko, N. N., Chkhalo, N. I., Pudonin, F. A., "Microfocus X-Ray Tubes with a Silicon Autoemission Nanocathode as an X-Ray Source," Bull. Lebedev Phys. Inst., 45, 1-5 (2018).

[14] Salashchenko, N. N., Chkhalo, N. I., and Dyuzhev. N. A., "Maskless X-Ray Lithography Based on Microoptical Electromechanical Systems and Microfocus X-Ray Tubes," J. Surf. Invest.: X-ray, Synchrotron Neutron Tech. 12 (5), 944-952 (2018).

[15] Basu A., Swanwick M. E., Fomani A. A., Velasquez-Garcia L. F., "A portable x-ray source with a nanostructured Pt-coated silicon field emission cathode for absorption imaging of low-Z materials," J. Phys. D: Appl. Phys., 48, 225501 (2015).

[16] Djuzhev, N. A., Makhiboroda, M. A., Preobrazhensky, R. Y., Demin, G. D., Gusev, E. E., and Dedkova. A. A., "Development and Study of a Conceptual Model of an X-Ray Source with a Field Emission Cathode," J. Surf. Invest.: X-ray, Synchrotron Neutron Tech. 11 (2), 443-448 (2017).

[17] Elfstrom, D., Guilhabert, G., McKendry, J., Poland, S., Gong, Z., Massoubre, D., Richardson, E., Rae, B. R., Valentine, G., Blanco-Gomez, G., Gu, E., Cooper, J. M., Henderson, R. K., and Dawson, M. D., "Mask-less ultraviolet photolithography based on CMOS-driven micro-pixel light emitting diodes," Opt. Express 17(26), 23522-23529 (2009).

[18] Bajt, S., "Molybdenum–ruthenium/beryllium multilayer coatings," J. Vac. Sci. Technol. A 18, 557-559 (2000).

[19] Chkhalo, N., Gusev, S., Nechay, A., Polkovnikov, V., Salashchenko, N., Schäfers, F., Sertsu, M., Sokolov, A., Svechnikov, M. and Tatarsky. D., "High reflective Mo/Be/Si multilayers for the EUV lithography," Opt. Lett. 42(24), 5070-5073 (2017).

[20] Krause, M. O., "Atomic radiative and radiationless yields for K and L shells," J. Phys. Chem. Ref. Data 8(2), 307-327 (1979).

[21] Menon R., Patel A., Gil D., Smith H. I., "Maskless lithography," Mater. Today 8(2), 26-33 (2005).

[22] Maihom, T., Sukuba, I., Janev, R., Becker, K., Mark, T., Kaiser, A., Limtrakul, J., Urban, J., Mach, P., and Probst, M., "Electron impact ionization cross sections of beryllium and beryllium hydrides," Eur. Phys. J. D, 67:2 (2013).

Downloaded From: https://www.spiedigitallibrary.org/conference-proceedings-of-spie on 03 Apr 2019
Terms of Use: https://www.spiedigitallibrary.org/terms-of-use

[23] Aphonin, V. P., Lebed', V. I., [Monte-Carlo method in x-ray spectrum analysis], Nauka, Novosibirsk, 6 (1989) (in Russian).
[24] http://henke.lbl.gov/optical_constants/filter2.html
[25] Kochetkov, A. A., Pestov, A. E., Lopatin, A. Ya., Tsybin, N. N., Chkhalo, N. I., "Conversion of electron energy to EUV radiation for thin film transmission targets," proceedings of workshop "Nanophysics and nanoelectronics - 2018" v.1, 452-453 , http://nanosymp.ru/UserFiles/Symp/2018_v1.pdf (2018) (in Russian).
[26] Blokhin, M. A., [Physics of X-rays], Gostechizdat, Moscow, 87 (1953) (in Russian).
[27] Chkhalo, N. I., Kluenkov, E. B., Lopatin, A. Ya., Luchin, V. I., Salashchenko, N. N., Sjmaenok, L. A., Tsybin, N. N., "Study of heat induced changes in elastic properties of multilayer Mo/$ZrSi_2$ membranes", Thin Solid Films 631, 93-98 (2017).
[28] Aruev, P. N., Barysheva, M. M., Ber, B. Ya., Zabrodskaya, N. V., Zabrodskii, V. V., Lopatin, A. Ya., Pestov, A. E., Petrenko, M. V., Polkovnikov, V. N., Salashchenko, N. N., "Silicon photodiode with selective Zr/Si coating for extreme ultraviolet spectral range," Quantum Electronics 42(10), 943-948 (2012).
[29] http://www.evex.com
[30] http://microanalyst.mikroanalytik.de/software.phtml
[31] http://montecarlomodeling.mcgill.ca

Downloaded From: https://www.spiedigitallibrary.org/conference-proceedings-of-spie on 03 Apr 2019
Terms of Use: https://www.spiedigitallibrary.org/terms-of-use